DOI: 10.1016/S1872-5805(21)60004-5

A review of charge storage in porous carbon-based supercapacitors

LUO Xian-you[1,2], CHEN Yong[1,2,*], MO Yan[2,*]

(1. *School of Material Science and Energy Engineering, Foshan University, Foshan* 528000, *China*;
2. *State Key Laboratory of Marine Resource Utilization in South China Sea, Hainan Provincial Key Laboratory of Research on Utilization of Si-Zr-Ti Resources, Hainan University, Haikou* 570228, *China*)

Abstract: Porous carbon-based electrode materials have been widely used in supercapacitors (SCs) because of their good physicochemical stability, high specific surface area, adjustable pore structure, and excellent electrical conductivity. The factors influencing their SC performance are analyzed, which include specific surface area, pore structure, surface heteroatoms, structural defects and electrode structure. The high surface area accessible to ions provides abundant active sites for their storage, while a suitable pore structure is important for the accommodation and diffusion of ions, thereby influencing the specific capacitance and rate performance of the electrodes. An appropriate pore size with a narrow distribution is required to increase the volumetric energy density while mesopores are favorable for ion transport, so a good balance between micro and mesopore volumes is important to improve both the energy and power densities of the SCs. Structural defects, surface heteroatoms and a rational electrode structural design all play significant roles in the capacitance performance.

Key words: Supercapacitors; Porous carbons; Specific surface area; Pore structure; Electrode structure

1 Introduction

Compared to rechargeable batteries, supercapacitors (SCs) are characterized by high-power density, short charge/discharge time, and long cycling life. However, SCs still suffer from low-energy density[1–3]. Basing on the different charge storage mechanisms, SCs are mainly categorized into pseudocapacitors and electric double layer capacitors (EDLCs)[4]. Pseudocapacitors store electric charges via fast and surface/near-surface controlled non-diffusion limited faradaic redox reactions[4,5], while EDLCs store electric charges at the electrode/electrolyte interface through physical adsorption/desorption processes of ions. The EDL capacitance (C) can obtained by Eq. (1)[6].

$$C = \frac{\varepsilon_r \varepsilon_0}{d} A \tag{1}$$

where ε_r, ε_0, d and A represent the permittivity of the vacuum (in $F \cdot m^{-1}$), relative dielectric constant of the electrolyte solution (no unit), distance from electrolyte ions to the electrode surface (in m), and ion-accessible surface area of the electrode material (in m^2), respectively.

Another critical performance parameter of SCs has to be with the energy density (E), which can be calculated by Eq. (2)[7].

$$E = \frac{1}{2} C V^2 \tag{2}$$

where C and V are the capacitance (in F) and applied voltage window (in V), respectively.

Obviously, high energy density can be obtained by improving the capacitance and electrochemical voltage window. The energy density of SCs in a specific electrolyte is mainly determined by the capacitance. In return, the capacitance performance of SCs affects their practical applications.

Standard SCs are generally made of two electrodes immersed in an electrolyte solution separated by a membrane. The electrode material is a crucial component in SCs since efficient electrochemical reactions at electrodes will yield good SCs performances. The most commonly used EDLCs are based on carbon materials due to their advantages in terms of low-cost, environmental friendliness, abundant sources, and excellent physicochemical stability. According to Eq. (1), a high ion-accessible surface area would generate satisfying capacitance in a certain

Received date: 2020-12-24; **Revised date:** 2020-12-28

Corresponding author: CHEN Yong, Ph. D, Professor. E-mail: ychen2002@163.com;
MO Yan, Ph. D, E-mail: myfriends66@163.com

Author introduction: LUO Xian-you, Ph. D candidate. E-mail: luoxianyou1990@163.com

electrolyte. As a result, numerous efforts have been devoted to obtaining high specific surface area porous carbon-based materials over the past few decades. The porosity of structure is indispensable for higher specific surface areas of carbon materials, which provide abundant electrochemical active sites for ions accumulation. Porous carbons, such as activated carbon, template carbon, porous graphene, and porous carbon nanotube are excellent candidates for EDLCs electrode materials due to their numerous advantages[1, 8, 9].

Some studies have noticed an anomalous increase in capacitance for porous carbon with a pore size below 1 nm. Therefore, both specific surface area and pore structure play important roles in the electrochemical performances of porous carbon electrodes[10, 11]. On the other hand, the specific surface area, pore size distribution, surface heteroatoms (or functional groups), and structural defects also impact the capacitance performance[12–15]. The introduction of heteroatoms in the carbon skeleton would mainly improve the electrical conductivity, wettability, and capacitance performance. Doped heteroatoms, such as O, N, S, F and B would change the surface chemical heterogeneity of carbon materials, thereby inducing additional pseudocapacitance through reversible redox reactions. In general, high capacitance porous carbons maybe possess elevated specific surface areas, suitable pore size distributions, and proper number of heteroatoms and structural defects[16–19].

In this mini-review, the influencing factors on porous carbon-based SCs are examined. These include the specific surface area, pore structure, surface heteroatoms, structural defects, and electrode design (Fig. 1). As mentioned above, high performance porous carbon-based SCs should take into account the synergic effect between different factors. Hence, such factors should be considered when designing and preparing porous capacitive carbons.

2 EDL theory in EDLCs

The classical plane EDL model has been described for the first time by von Helmholtz[20]. He proposed that electric charges accumulate at the electrode/electrolyte interface through electrostatic adsorption (Fig. 2a). Gouy and Chapman then suggested the diffusion layer model by considering the non-uniform distribution of ions induced by the diffusion of ions and dipole movement of solvent molecules driven by thermal fluctuation (Fig. 2b)[21, 22]. In this model, the thickness of the diffusion layer (λ_D) can be presented by Eq. (3), and the capacitance (C_D) can be described by Eq. (4).

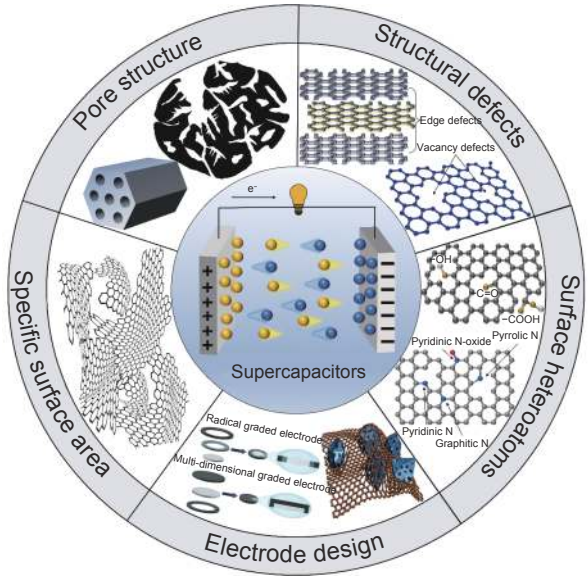

Fig. 1 Influencing factors on the electrochemical performances of porous carbon-based SCs. Reprinted with permission.

$$\lambda_D = \sqrt{\frac{\varepsilon_0 \varepsilon_r RT}{2(zF)^2 C_0}} \tag{3}$$

$$C_D = \frac{\varepsilon_0 \varepsilon_r}{\lambda_D} \cosh\left(\frac{zF\psi}{2RT}\right) \tag{4}$$

where ε_0, ε_r, R, T, z, F, C_0 and ψ refer to the vacuum dielectric constant (in $F \cdot m^{-1}$), relative permittivity of the electrolyte solution (no unit), ideal gas constant (in $J \cdot mol^{-1}$), absolute temperature (in K), Faraday constant (in $C \cdot mol^{-1}$), concentration of the electrolyte solution (in $mol \cdot m^{-3}$), and electrical potential (in V), respectively.

Later, Stern introduced an additional compact layer by considering the actual ions size based on Gouy-Chapman model (Fig. 2c)[23]. In this case, the capacitance may be described according to Eq. (5)

$$\frac{1}{C_{DL}} = \frac{1}{C_H} + \frac{1}{C_D} \tag{5}$$

where C_{DL}, C_H and C_D refer to the capacitance of EDL, Helmholtz layer and diffusion layer, respect-

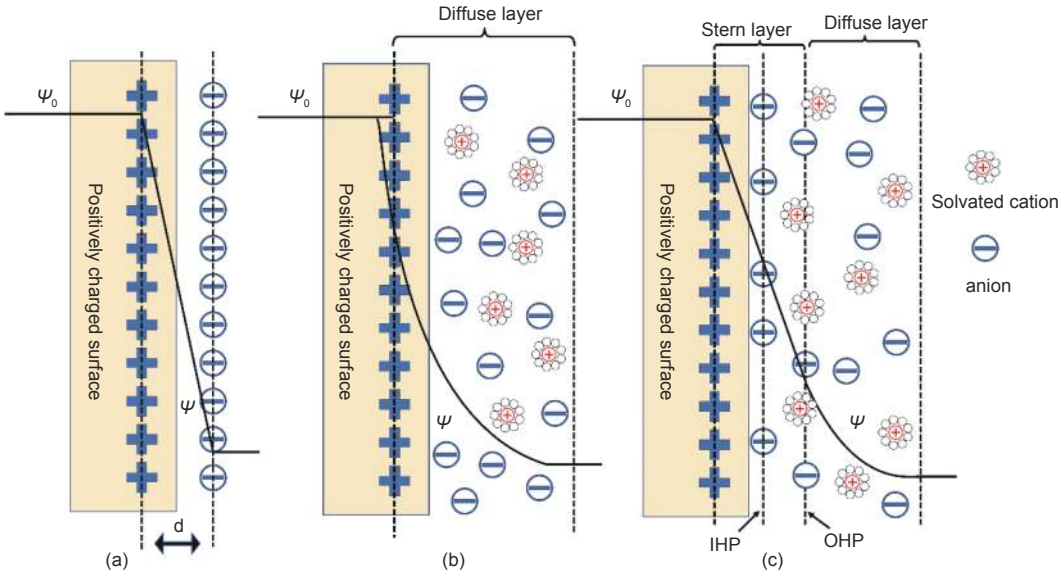

Fig. 2　Different EDL models: (a) Helmholtz, (b) Gouy-Chapman and (c) Stern. d presents the electric double layer distance in Helmholtz model[23]. Ψ_0 and Ψ are potentials at the electrode surface and electrode/electrolyte interface, respectively. Reprinted with permission.

ively.

However, Stern model still suffers from limitations in highly concentrated electrolytes or ionic liquids since it ignores the effects of ions interaction[9, 24]. To solve this issue, a Landau-Ginzburg-Type continuum theory was developed by considering the EDL structure in ionic liquids, different from that used for solvent-containing electrolytes. In ionic liquids, the absence of solvent molecules for screening cations and anions would lead to strong ions interactions. In these conditions, the EDL exhibits an overscreening effect under lower potential (0.26 V), while a crowding effect is observed under larger polarization potential (2.6 V) thanks to different ionic interactions (Fig. 3)[25].

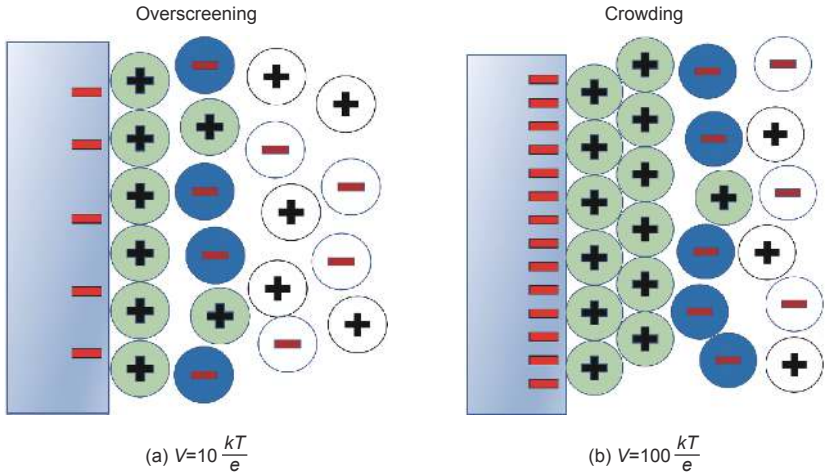

Fig. 3　(a) Overscreening effect at moderate voltage and (b) crowding effect at high voltage[25]. Reprinted with permission.

3　Influencing factors on supercapacitance of porous carbon

Porous carbon is an excellent candidate for SCs electrode materials due to its elevated specific surface area, adjustable pore structure, low-cost, environmental friendliness, and abundant resources. All carbon-containing precursors, such as biomass or their derivatives could be converted into porous carbon by vari-

ous synthetic routes like template, carbonization, and activation[26–31]. For instance, natural or synthetic materials, such as wood[32, 33], rice husk[34], coconut shells[35], fossil fuel[36], and polymers[37, 38] can be utilized as carbon precursors to prepare activated carbon by physical and/or chemical activation under inert atmosphere through the selective oxidation and/or etching in water steam[39, 40], CO_2[41, 42], KOH[43, 44], NaOH[45, 46], or $ZnCl_2$[47, 48]. Obtained porous carbons by these routes often possess superior specific surface area and well-developed porous structure after chemical activation. However, the lower energy density of the resulting SCs severely hinders their widespread applications when compared to rechargeable batteries. Hence, improving the specific capacitance and energy density would be of great importance for the next generation of SCs. To this end, factors like the specific surface area, pore structure, surface heteroatoms, structural defects, and electrode structure should be considered since they determine the electrochemical performances of porous carbon used in SCs.

3.1 Specific surface area

According to Eq. (1), a linear correlation between the specific capacitance and specific surface area might be obtained to increase the specific surface area of porous carbons, and thereby effectively improving the specific capacity. However, no linear correlation between the specific capacitance and specific surface area has so far been obtained experimentally[49–51]. Theoretically, by considering a mean value of 20 $\mu F \cdot cm^{-2}$ for EDL capacitance and a porous carbon with BET specific surface area of 920 $m^2 \cdot g^{-1}$, a maximum theoretical specific capacitance reaching up 182 $F \cdot g^{-1}$ could be obtained. Nevertheless, the actual specific capacitance, in this case, reached only 80 $F \cdot g^{-1}$. This meant that only 44% BET specific surface area contributed to the capacitance value[52]. As a result, increasing the specific surface area of porous carbons would not significantly enhance the specific capacitance value. On the other hand, it has to be noted that most BET specific surface areas of porous carbons have been estimated by the adsorption/desorption isotherms of a certain probe gas, such as N_2, Ar, or CO_2. As a result, a fraction of ion-inaccessible surface would exist due to the sieving effect of pores toward ions[53]. However, some pore channels cannot absorb ions during the actual charge/discharge processes to form EDL since the ionic size does not match the pore size. On the other hand, high specific surface areas could improve the gravimetric specific capacitance by providing more ions adsorption sites. Nonetheless, excessively high specific surface areas would lead to large pore volume induced by micropores, thereby decreasing the density and volumetric specific capacitance of porous carbon. Thus, a crucial balance problem between the specific surface area and pore structure exists and should be solved to yield superior capacitance values. In other words, appropriate specific surface area and volume energy density should also be considered as critical factors when dealing with capacitive carbons.

3.2 Pore structure

3.2.1 Effect of basic pore structure

Factors like the specific surface area and pore structure characteristics (pore size, pore size distribution, and pore shape) are also crucial factors influencing the capacitance performances of porous carbons. The pore structure impacts the charge transfer and ions transport, thereby severely affecting the capacitance and rate performances. So far, the relationships between ions and pore size have been explored[50, 53, 54]. Some studies suggested that pore sizes smaller than those of solvated ions will not contribute to EDL capacitance. However, others indicated that microporous carbons with a smaller pore size (<1 nm) would deliver superior capacitance in various electrolytes with larger solvated ions. For example, Chmiola et al. reported an anomalous increase in capacitance of carbide-derived carbons (CDCs) with pore size below 1 nm (Fig. 4a). For pore size twice larger than that of solvated ions, the compact layers of solvated ions residing on both adjacent pore walls highly contributed to the capacitance (Fig. 4b). For pore size smaller than twice that of solvated ions, the EDL capacitance decreased due to the decline in compact ions layers from adjacent pore walls and accessible EDL sur-

face area (Fig. 4c). As the pore size further reduced to the size of desolvated ions, a striking increment in capacitance was observed. The reason for that has been associated with the distorted solvation shell, which allowed the center of the ions to move closer to the pore walls (Fig. 4d)[10]. Raymundo-Pinero et al. obtained similar results with microporous carbon both in aqueous and non-aqueous electrolytes. Note that pore filling was more effective for the formation of EDL at pore size around 0.7 nm in aqueous electrolytes and 0.8 nm in organic electrolytes[55]. Such increase in EDL capacitance for sub-nanometer pores (<1 nm) broke the traditional viewpoint related to electrolyte ions adsorption and EDL formation in porous carbons[4]. As a result, more attention has been focused on exploring the sub-nanometer porous carbon. For instance, exfoliated graphene (EG)-mediated graphene oxide (GO) films (EGM-GO) with tunable interlayer spacing were obtained by vacuum filtration of aqueous EG and GO dispersion mixed precursors at different mass ratios. A precise adjustable slit pores size was achieved by tuning the interlayer spacing of EGM-GO film. For pore size of EGM-GO film matching the diameter of the electrolyte ions, the most effective pore utilization was obtained for optimizing the volumetric capacitance[56].

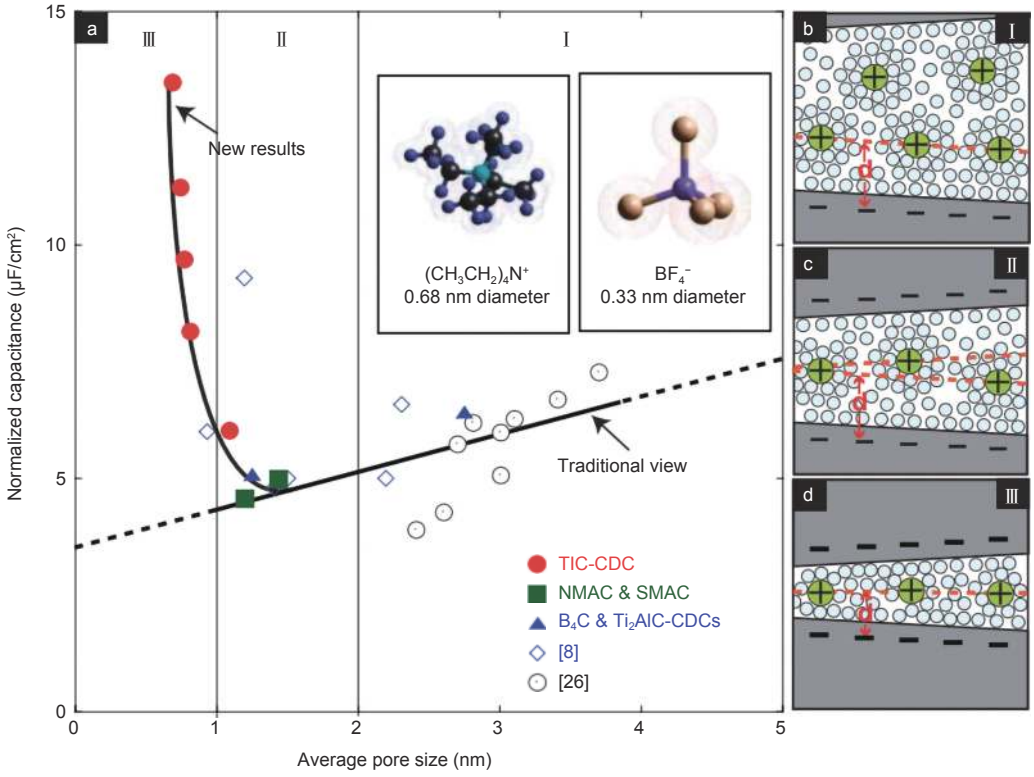

Fig. 4　(a) Correlations between normalized capacitance and average pore size in an electrolyte containing 1.5 mol L^{-1} $TEABF_4$ dissolved in ACN. Solvated ions residing in pores with a distance between adjacent pore walls: (b) >2 nm, (c) 1—2 nm, and (d) <1 nm[10]. Reprinted with permission.

The capacitance in sub-nanometer pores can be improved by ions desolvation effects[4, 57, 58], as confirmed by experiments and theoretical computations. For example, changes in EDL capacitances were recorded by measuring the current responses of negative and positive electrodes with different sub-nanometer carbons with pore sizes smaller than those of solvated ions. The reduction in pore size lead to an increment in the number of desolvated ions, thereby improving the capacitance (Fig. 5)[57]. To clarify the capacitance contribution of sub-nanometer pores, a model based on graphene oxide with tunable interlayer spacing was also designed to correlate the capacitance to pore size by interlayer regulation, meaning *in-situ* tuning the interlayer of graphene oxide paper. A maximum specific capacitance was achieved when the interlayer distance matched well the desolvated ions[59]. Similarly, a partial desolvation effect was no-

ticed by cyclic voltammetry combined with *in-situ* electrochemical quartz crystal microbalance methods in EMITFSI/ACN electrolyte. The adsorption of EMI^+ cations on carbide-derived carbons (CDCs) with different average pore sizes of 1 nm and 0.65 nm led to 3—4 and 1—2 solvent molecules arounding EMI^+, respectively. Thus, the desolvation effect increased as pore size decreased from 1 nm to 0.65 nm[60]. Data from *in-situ* small-angle X-ray scattering and Monte Carlo simulations indicated that Cs^+ and Cl^- ions in nanoporous carbon with partial desolvation effect in water solution tightly attached to the aqueous solvation shell could effectively inhibit ion desolvation in nanoporous carbon[58].

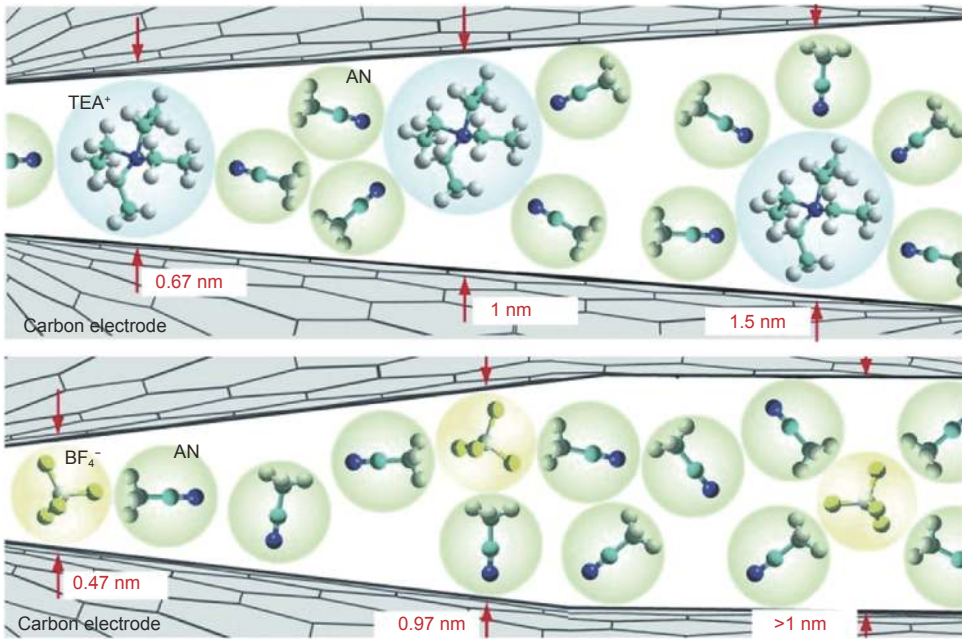

Fig. 5 Geometric confinement of ions in small pores. Ion size: TEA^+ (0.67 nm) and BF_4^- (0.47 nm)[57]. Reprinted with permission

To prevent the influence of the solvation shell, the relationships between normalized capacitance and pore size of various CDCs were investigated in solvent-free EMITFSI ionic liquid (Fig. 6). A maximum capacitance was recorded for ions size close to the pore size[11]. Note that high capacitance could be gained when ions were confined in the same dimension pores[61]. Therefore, the optimal capacitance should be fulfilled as long as the pore size of porous carbon matched the desolvated ions size.

The hydration behaviors of various electrolyte ions in sub-nanopores carbon have also been investigated by molecular dynamics (MD) simulations[62, 63]. The temperature effect on hydration ions in CNTs suggested different hydration behaviors of Li^+, K^+, Na^+, F^- and Cl^- residing in CNTs at 298-683 K. Especially, the H_2O molecules in coordination shell of K^+ revealed ordered structures as temperature increased in CNTs with an effective diameter of 1 nm. This led to an enhancement effect of ionic hydration different from that in bulk solution. However, the other four ions did not manifest such behavior in CNTs with an effective diameter of 0.73-1 nm. This can be explained by the agreement between the size of an easily distorted K^+ coordination shell and pore size[64]. Later, the “superionic state” concept was proposed to explain the anomalous capacitance behavior of ions in nanopores. This involved two aspects. The first dealt with the image forces from the metallic properties of nanoporous carbon, which weakened the electrostatic interactions between ion-ion pairs in nanopores, and thereby breaking the Coulombic order of ions and enabling the same ions to occupy the nanopores. The second had to be with the difference in free energy, which urged ions transmission from the bulk of the electrolyte solution into the inner nanopores[65]. In the superionic state, the Coulombic order of ionic liquids confined in nanopores was broken, meaning the same

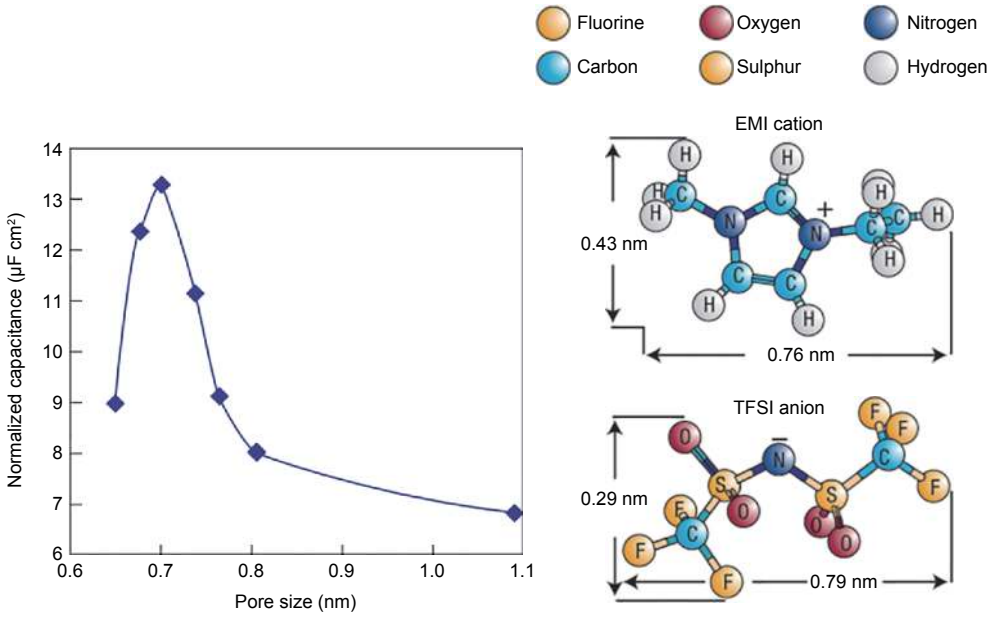

Fig. 6　Plots of specific capacitance normalized by SSA as a function of average pore size obtained for various CDC electrodes in neat EMITFSI ionic liquid[11]. Reprinted with permission.

charge of ions neighboring each other due to image charges induced by pore walls screening of electrostatic interactions. The existence of superionic state of ionic liquid ions confined in nanopores was experimentally validated by small-angle X-ray scattering. Bilayer confinement of ionic liquid ions in 1 nm pores did not break the Coulombic order since additional layers could form on each carbon wall. By contrast, monolayer confinement in 0.7 nm pores broke the Coulombic order, thereby forming cation-anion pairs[66].

On the other hand, SCs with excellent capacitance performances commonly possess high-energy and high-power density. However, the pore filling process of ions is extremely complicated. Besides pore size, pore size distribution, pore shape, and pore regularity all affect the electrochemical properties of porous carbons[1, 67]. For pore size distribution, a non-monotonic function exists between the energy density and pore size of monodisperse porous carbons. The optimal pore size delivering the maximal energy density increased with the applied potential and showed saturation at high potentials[68]. Narrowing the pore size distribution would raise the energy density, leading to monodisperse porous carbons with appropriate pore sizes for ideal SCs electrode materials. The pore aspect ratio can be used to evaluate the pore structure of ordered mesoporous carbons, defined as the ratio between the pore length and pore diameter. The ions transfer kinetics process can be described by Eq. (6) based on the classical electrochemistry theory[69].

$$\tau = \frac{L^2}{D} \tag{6}$$

where τ, L and D represent the ions transport time, length and coefficient, respectively.

Accordingly, shorter and larger pores would lead to better ions transport behavior. In terms of pore regularity reflecting the content of pore defects[70], more pore defects would lower the regularity of porous carbon but higher pore regularity should improve the ions transfer kinetics since pore defects can scatter ions. Thus, monodisperse pores with adaptable pore size would increase the capacitance performances of porous carbons[1, 68].

In general, planar pore shape favor the fast transmission of ions, while disordered or curved pore architecture severely hinders the ions delivery[14, 71]. Some studies suggested that pore geometry and pore mouth size would all affect the charge redistribution. Among cone-, inverted cone- and cylindrical-shaped pores with the same resistance and capacitance, cone-shaped pores exhibited the maximal charge storage capacity[72]. Finally, the spatial geometry and dimen-

sion of ions also impact the adsorption process due to the ions sieving effect. For instance, Cl^- and ClO_4^- can be absorbed on carbon molecular sieve, while SO_4^{2-} cannot be adsorbed[73].

The good energy density and power density of porous carbon electrode materials are advantages for high capacitance and fast ions transfer kinetics. As a result, carbons with high specific surface areas and hierarchical pores with enhanced supercapacitance performances have been explored[1, 74, 75–80]. Hierarchically porous carbons with micro-/meso-/macro-pores (size <2 nm/2 nm-50 nm/>50 nm) could provide plentiful chemically active sites to accommodate ions, as well as abundant multiple channels for ions transmission and affluent reservoirs space for ion-buffering. For example, microporous carbon fiber electrode materials showed lower rate performances when compared to micro-/meso-porous aerogels carbon due to the latter possess hierarchical porous structure composed of micro- and meso-pores[73].

3.2.2 Endohedral/exohedral capacitor models

Several theoretical models based on surface curvature effects have been proposed to gain a better understanding of the charge storage mechanism of porous carbon, as well as the enhanced capacitance behavior in sub-nanometer pores. The classical 2D planar EDL model is generally limited as it cannot explain the mechanism of charge storage in 3D porous carbon due to the non-consideration of surface curvature and porous effects[9]. Porous carbon possesses various pores endohedral shapes, such as slit, cylindrical and spherical pores, as well as exohedral pores between carbon nanoparticles like CNTs and carbon onions[81].

Huang et al. proposed the endohedral capacitor model to describe porous carbon-based EDLCs by considering endohedral pore curvatures[82, 83]. In this model, an electric double-cylinder capacitor (EDCC) model (Fig. 7a) was designed by assuming cylindrical-shaped mesopores, where ions could enter the mesopores and further approach the pore walls to form EDCC under electric polarization. The corresponding EDCC capacitance can be described by Eq. (7a), and the normalized capacitance with surface area A can be given by Eq. (7b):

$$C = \frac{2\pi\varepsilon_r\varepsilon_0 L}{\ln(b/a)} \tag{7a}$$

$$C/A = \frac{\varepsilon_r\varepsilon_0}{b\ln[b/(b-d)]} \tag{7b}$$

where L, b, a and d represent the pore length, radii of the outer cylinders, radii of the inner cylinders and distance between the center of counter ions and the pore walls, respectively.

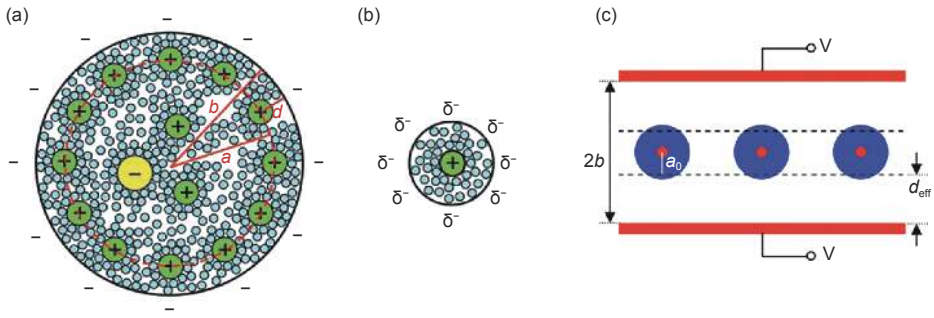

Fig. 7 Schematic plots of (a) electric double-cylinder capacitor with mesopores and (b) electric wire-in-cylinder capacitor with micropores[83]. (c) Schematic plot of sandwich capacitor[84]. Reprinted with permission.

For micropores, an electric wire-in-cylinder capacitor (EWCC) model was constructed by assuming cylindrical micropores (Fig. 7b). The solvated or desolvated ions would enter the micropores to line up, forming EWCC. The capacitance can be described by Eq. (8):

$$C/A = \frac{\varepsilon_r\varepsilon_0}{b\ln(b/a_0)} \tag{8}$$

where b and a_0 are the radius of micropore and inner cylinder formed by counter ions, respectively.

Feng et al. proposed a sandwich capacitor model by considering the presence of slit-shaped pores (Fig. 7c)[84]. The molecular dynamics simulations

showed that K^+ ions were enclosed in slit-shaped micropores with pore widths between 0.1 and 1.47 nm to form EDL through ions hydration and water-water interactions. The capacitance of sandwich capacitors can be expressed according to Eq. (9):

$$C/A = \frac{\varepsilon_r \varepsilon_0}{b - a_0} \tag{9}$$

where b and a_0 refer to the half of the slit-shaped pore width and effective ion radius of the counter ions.

In general, exohedral capacitance forms on outer surfaces of carbons, including zero-dimensional carbon onions or one-dimensional carbon nanotube arrays[81, 83]. For carbon onions, solvated counterions approaching the carbon surface can be approximated as solid spheres to form exohedral electric double-sphere capacitors (xEDSCs, Fig. 8a). Similar to CNTs, solvated counter ions form exohedral electric double-cylinder capacitors (xEDCCs) on the outer walls of CNTs (Fig. 8b). The cross-sections of the two exohedral capacitors are schematically summarized in Fig. 8c, and the corresponding capacitance of xEDSC model is provided by Eq. (10a) and Eq. (10b). Accordingly, the capacitance of xEDCC model can be expressed by Eq. (11).

$$C = \frac{4\pi\varepsilon_r\varepsilon_0 ab}{b - a} \tag{10a}$$

$$C/A = \frac{\varepsilon_r\varepsilon_0(a + d)}{ad} \tag{10b}$$

$$C/A = \frac{\varepsilon_r\varepsilon_0}{a\ln[(a + d)/a]} \tag{11}$$

where a, b and d are the radius of the inner sphere/cylinder charge layer, outer sphere/cylinder charge layer and effective double-layer thickness, respectively.

The endohedral and exohedral capacitor models considering surface curvature effects showed agreement with the experimental data to some extent. The correlations between the normalized capacitance and particle/pore size of endohedral capacitors and exohedral capacitors are depicted in Fig. 9[81].

3.2.3　Physisorption techniques

The specific surface area and pore size distributions are two fundamental parameters of porous carbons with vital roles in specific capacitance and energy density. High specific surface area and appropriate pose size distribution would improve the capacitance properties. However, overlarge pore volume caused by excessive pore size may generate unfavorable volumetric specific capacitance. Hence, correctly obtaining porous carbons with a high specific surface area and suitable pore size would be of great importance for better capacitance values.

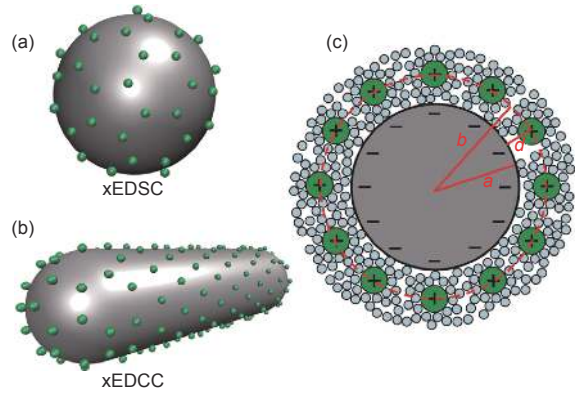

Fig. 8　(a) Plots of 0D spheres and (b) 1D tubes with counter ions approaching the outer surface. (c) Schematic plot displaying the cross-section of an exohedral capacitor[81]. Reprinted with permission.

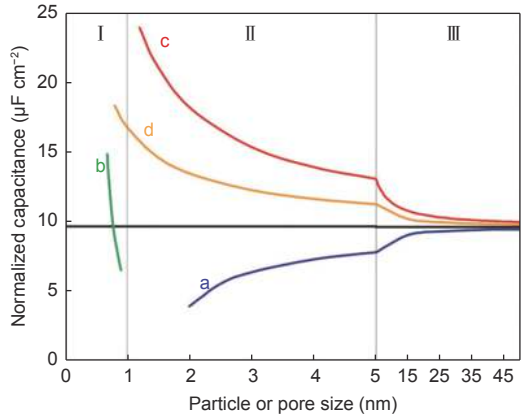

Fig. 9　Correlations between normalized capacitance and particle/pore size of endohedral capacitors. Note that curves a and b represent the mesoporous and microporous carbons. For exohedral capacitors, the curves c and d represent 0D spheres and 1D tubes. The black line represents parallel-plate capacitor[81]. Reprinted with permission.

Physisorption is effectively and widely applied to characterize these two parameters. In this process, gas probe molecules are used to obtain the adsorption/desorption isotherms followed by analyses of the specific surface area and pore size distributions[85, 86].

N_2, Ar and CO_2 are the most commonly employed gas probe molecules for evaluation of the specific surface area and pore size distributions of por-

ous materials. Though N_2, Ar and CO_2 have similar molecular dimensions, such as 0.36, 0.34 and 0.33 nm, they differ in adsorptive behaviors[86]. This might be related to factors like the interaction between the gas probe molecules and solid surface of adsorbents, as well as the chemical composition and surface functional groups of the solid surface. As a result, different solid surfaces would require appropriate gas probe molecules for assessment of the physisorption. Moreover, the adsorption measurements of the same solid surface vary with the nature of gas probe molecules. Therefore, proper physisorption gas could provide a comprehensive and accurate pore structural analysis.

In general, N_2 at 77 K is employed as a popular gas probe molecule for both micro- and meso-porous analysis. However, the existence of quadrupole in N_2 molecule interacts with the surface functional groups and exposes ions, thereby affecting the orientation of adsorbed N_2 molecules on the solid surface and micropore filling pressure[85]. By contrast, Ar at 87 K does not undergo specific interactions with surface functional groups since Ar has no quadrupole properties. Compared to N_2 (77 K), the elevated relative pressure of Ar (87 K) accelerates the diffusion of Ar molecules and shortens the equilibration time when filling micropores with dimensions of 0.5—1 nm. On the other hand, a well-known limited diffusion problem exists at low temperatures (87 K for Ar and 77 K for N_2), severely preventing Ar or N_2 molecules from entering the ultra-micropore with a pore size of ~0.45 nm[87]. Alternatively, CO_2 at 273 K is used to assess the specific surface area and pore size distribution of ultra-micropore carbons (as small as 0.45 nm) due to its fast diffusion at higher operating temperatures[88]. However, CO_2 possesses a quadrupole moment, severely affecting its adsorption behavior when assessing porous materials containing oxygen functionalities and other oxidizing materials[89]. In sum, Ar is an appropriate gas probe molecule for assessing porous carbons with or without surface functional groups.

Hence, choosing appropriate models and algorithms for assessing the specific surface area and pore size distribution is vital for obtaining correct values. The classical BET equation is mainly applicable to nonporous or mesoporous surface area analysis but not to microporous materials[90]. In this situation, multi-points BET method can be used to analyze porous materials containing micropores[91].

Numerous models have also been developed to obtain the pore size distribution of porous materials. The Barrett-Joyner-Halenda (BJH) method is often utilized to analyze the pore size distribution of mesoporous materials. Note that this equation is based on the modified Kelvin equation and capillary condensation phenomenon[92]. However, BJH does not apply to microporous materials due to micropore filling process. Microporous materials usually adopted Dubinin-Radushkevic (DR)[93, 94], Horvath-Kawazoe (HK)[95], and Saito-Foley (SF)[96] to calculate the micropore size distribution in early years. However, both the experimental and theoretical results revealed differences between the thermodynamic properties of free fluid and confined fluid, leading to non-applicability of classical BJH, DR, HK and SF methods[97]. Additionally, non-local density functional theory (NLDFT)[98, 99], quenched solid-state density functional theory (QSDFT)[100, 101], and 2D-non-local density functional theory (2D-NLDFT)[102] have been developed for porous structural analysis. These methods are based on computational technology, suggesting that density functional theory (DFT) can provide more accurate and comprehensive pore size distribution assessment when compared to classical and macroscopic methods[85]. The NLDFT describes the fluid state in confined pores by considering the fluid-fluid and fluid-pore wall interactions and molecular potential energies[90]. NLDFT is based on an independent slit-shaped pores model with ideal graphitic walls, which ignores the influence of surface heterogeneity of pore walls in actual porous materials. This induces artificial peaks in pore size distribution profiles. Furthermore, QSDFT has been developed to accurately calculate the pore size distributions by considering heterogeneous solid surfaces with corrugated amorphous walls[103]. By ana-

logy, the standard slit-shaped pore model in NLDFT was employed to form 2D-NLDFT model by introducing energetical and/or structural heterogeneity to pore walls surface[102]. This eliminates the presence of typical artifact peaks observed in homogeneous slit-shaped pore model.

Although QSDFT is widely used to assess the pore size distribution of porous materials, it still suffers from apparent artifact peaks in pore size distribution profiles when assessing unclosed adsorption/desorption isotherms. In other words, the tensile strength effect induces an artifact peak around 2.8 nm when the desorption branch of the isotherm is employed to calculate the pore size distribution. Hence, the adsorption branch can be employed to estimate the pore size distributions[104].

3.3 Structural defects

Structural defects, including vacancies, basal-, edge-, and defect-surfaces in carbonaceous materials can be used as electrochemically active sites for ions adsorption and improvement of the capacitance performance[13, 105]. Previous reports have confirmed the existence of abundant electrochemically active sites on the edge-surfaces of carbon materials. These sites are useful for generating high capacitance when compared to basal-surfaces[106–108]. In this respect, the edge-surfaces of platelet or herringbone carbon nanofibers (CNFs) showed 3-5-fold superior capacitance values than basal-surfaces of tubular CNFs. On the other hand, graphitization could transform edge-surfaces of platelet CNFs into domelike basal-surfaces. Such a process resulted in a capacitance decrease from 12.5 $F\cdot g^{-1}$ to 3.2 $F\cdot g^{-1}$. However, the use of chemical oxidation raised again to increase the capacitance to 5.6 $F\cdot g^{-1}$ by recovering the edge-surfaces after removal of the curved basal-surfaces[107]. On the other hand, single-layer graphene edge exhibited 4-fold higher capacitance, faster electron transfer rate, and stronger electrochemical activity than basal-surfaces[109].

Various strategies have been utilized to introduce structural defects on surfaces of carbonaceous materials. Processes like activation, heteroatoms insertion and subsequent removal treatment have been effectively employed to prepare defective carbons[110,111]. For example, defective carbon from macadamia nut shells was synthesized by nitrogen doping. The removal of nitrogen atoms led to the formation of structural defects in the carbon skeleton[111]. Defective carbon from lotus leaves was obtained through a two-step activation approach. The first step of HNO_3 activation introduced nitrogen atoms in the carbon skeleton, while the second step of KOH activation promoted the removal of nitrogen atoms, leading to the generation of some defects and pores[110]. Defective carbon nanosheets from syzygium cumini leaves were successfully prepared through $NaHCO_3$ activation to yield moderate levels of structural defects, useful for inducing abundant electroactive sites for ions storage[112].

Ball-milling has also been used to create structural defects in carbons layers, especially graphite and expanded graphite[113, 114]. After 100 h ball-milling, the crystallite size of expanded graphite decreased gradually from 15.4 nm to 11.3 nm, creating numerous in-plane defects[114]. Similarly, the defect density and sp^2 carbon cluster size of dense graphene blocks can be tailored through ball-milling process, thereby generating high gravimetric/volumetric capacities and excellent rate performance in Na-ion capacitor. The abundant structural defects after ball-milling generated dense graphene blocks with excellent volumetric capacity and rate performance when compared to expanded graphene and graphite. Therefore, defects modulation significantly affect energy storage[115]. Also, previous studies found that basal-, edge-, and defect-surfaces of carbon graphitic layer delivered different capacitance contributions estimated to 0.04 $\mu F\cdot cm^2$, 1.65 $\mu F\cdot cm^2$ and 7.95 $\mu F\cdot cm^2$, respectively. The largest values of capacitance were obtained in the presence of defects (Fig. 10). Consequently, reasonable regulation of defects could significantly improve the capacitance performance of carbon-based materials[13].

3.4 Surface heteroatoms

The introduction of surface heteroatoms could also influence the electrochemical properties of carbon materials. The species and concentration of surface heteroatoms may be adjusted by the preparation process or proper thermal and/or chemical treatments.

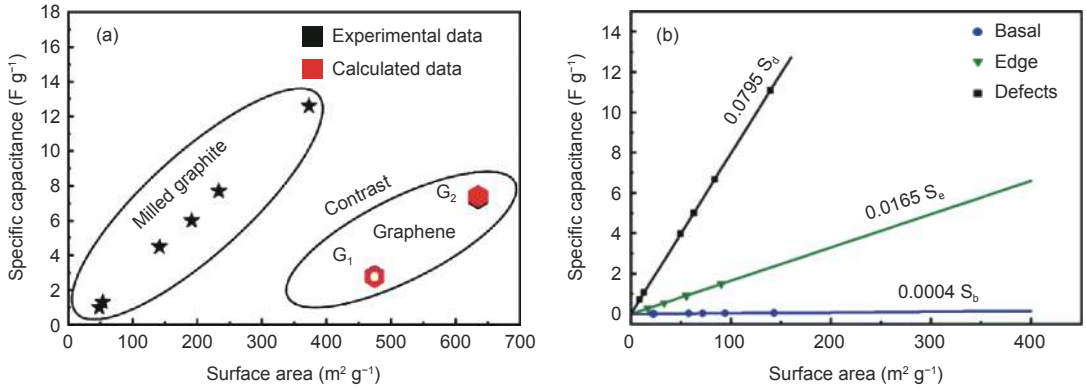

Fig. 10 (a) Variation in surface area with a specific capacitance of milled-graphite and graphene. (b) Correlations between three types of surface area and specific capacitance[13]. Reprinted with permission.

The introduction of surface heteroatoms in carbon skeleton often changes the electrical conductivity, wettability, and capacitance performance of carbon materials. In particular, the presence of heteroatoms induces surface chemical heterogeneity, which determines the chemical properties of carbon materials[116]. Heteroatoms, such as oxygen (O), nitrogen (N), phosphorous (P), sulfur (S), fluorine (F) and boron (B) doped carbon materials can be derived from precursors materials containing the corresponding heteroatoms or introduced by post-treatment/activation processes[12, 30].

Oxygen doping by means of oxygen functional groups maybe obtained through the pyrolysis of oxygen-containing precursors such as most biomass[117, 118], chemical alkali activation (KOH or NaOH), or chemical reagents (HNO_3[119, 120], $(NH_4)_2S_2O_8$[121] and H_2O_2[116]) post-treatment. In general, oxygen functional groups, such as hydroxy, carboxyl, and carbonyl can improve the surface wettability and increase the capacitance performance of SCs in aqueous electrolytes[121, 122]. The introduction of such pseudocapacitance maybe performed in basic electrolytes through redox reactions of oxygen functional groups (Eqs. (12-14))[123, 122].

$$>C-OH+OH^- \leftrightarrow >C=O+H_2O \quad (12)$$

$$>C=O+e^- \leftrightarrow >C-O^- \quad (13)$$

$$>COOH+OH^- \leftrightarrow -COO^-+H_2O \quad (14)$$

In 1 mol/L H_2SO_4 electrolyte, quinone-coated onion-like carbon showed higher specific capacitance (264 $F\cdot g^{-1}$) than uncoated onion-like carbon (30 $F\cdot g^{-1}$). The reason for this was linked to the redox reaction of quinone groups (—C═O + H^+ + e^- ↔ —C—O—H). Hence, oxygen functional groups can improve the specific capacity[124]. Additionally, appropriate oxygen functional groups like carboxyl and carbonyl may considerably contribute to the capacitance improvement in aqueous electrolytes, while this may not be beneficial in organic electrolytes. The reason for this is associated with the modifying bulky oxygen functional groups on the carbon surface, which may block the pores and hinder ions transport[121]. In this regard, removal of unstable surface oxygen functional groups can improve the electrochemical performances of porous carbons in organic electrolytes in terms of lower self-discharge and leak current, as well as better cycling stability[125].

Nitrogen heteroatom is also widely explored to improve the electrochemical reactivity of carbon materials.[14, 30, 126]. Nitrogen in carbonaceous materials could afford extra electroactive sites due to its electron-donor properties, as well as increase the surface polarity, wettability, and electrical conductivity through the change in the valence electron orbital energy levels of neighboring carbon atoms and creation of defects[126]. Nitrogen atoms exist in N-doped-carbons in the form of pyrrolic-N, pyridinic-N, quaternary-N, and pyridinic-N-oxide. The pyrrolic-N and pyridinic-N provide pseudocapacitance by redox reactions, while quaternary-N and pyridinic-N-oxide accelerate the electron transfer and improve the electrical conductivity[14]. The incorporation of nitrogen might improve the wettability and hydrophilicity of carbon materials, thereby increasing the accessible active surface areas for ions adsorption and storage. Therefore, nitrogen-doped carbon materials often

show excellent capacitance performance. For example, porous carbon doped with 21.7 at.% nitrogen to form fully electrochemically active nitrogen species, such as pyrrolic-N, pyridinic-N and oxidized-N delivered superior energy density of 36.8 $Wh \cdot kg^{-1}$ at 2 $kW \cdot kg^{-1}$, as well as power density of 38 $kW \cdot kg^{-1}$ at 25.7 $Wh \cdot kg^{-1}$[127]. A nitrogen-rich cocoon silk derived carbon was successfully doped with 6.05 wt.% nitrogen content to yield mainly dominated electroactive pyrrolic-N and pyridinic-N after g-C_3N_4 mediation. The resulting material exhibited a high capacitance of 392 $F \cdot g^{-1}$ at 1 $A \cdot g^{-1}$ and an outstanding rate performance of 222 $F \cdot g^{-1}$ at 20 $A \cdot g^{-1}$[128].

Other heteroatoms, such as S, P, B, and F have also been extensively studied to regulate the surface properties and improve the electrochemical properties of carbon materials[129, 12, 15]. However, dual or more heteroatoms co-doped carbon materials are more effective in most situations since they can deliver excellent capacitance performances than single atom doped-materials due to synergy among different heteroatoms[130]. For instance, N and F co-doped carbon microspheres (CM-NF) with ultra-high volumetric capacitance (521 $F \cdot cm^{-3}$) and excellent cycling stability were successfully prepared. The incorporation of F in CM-NF enhanced the volumetric capacitance by over 100% when compared to that obtained without F-doping, and exhibited outstanding cycling performance without any capacity loss after 10 000 cycles[131]. Moreover, N and F co-doped hierarchically porous carbon from polyaniline illustrated superior specific capacitance of 291 $F \cdot g^{-1}$ at 0.5 $A \cdot g^{-1}$, a value higher than that obtained without F-doped of 238 $F \cdot g^{-1}$. This material also exhibited 95.5% capacitance retention after 10 000 cycles[132]. N and B co-doped porous carbons from citric acid showed elevated specific capacitance of 268 $F \cdot g^{-1}$ when compared to the value recorded without N and B co-doped (111 $F \cdot g^{-1}$ at 2 $mV \cdot s^{-1}$). This was attributed to N and B heteroatoms that led to enhanced wettability between the electrode and electrolyte interface, thereby resulting in a pseudocapacitive effect[133]. Porous carbon from phytic acid provided abundant active sites after co-doping with P and N atoms, leading to excellent gravimetric and volumetric capacitance of 317 $F \cdot g^{-1}$ (482 $F \cdot cm^{-3}$) at 1 $A \cdot g^{-1}$ in 1 mol/L H_2SO_4 electrolyte[134]. Other heteroatoms used for co-doping porous carbons include N/P[135, 136], N/O[137, 138], N/S[139, 140], F/N[141], B/N[142, 143], and N/O/S/Cl[144]. Such co-doping with these species led to excellent comprehensive SCs capacitance performances due to the change in surface properties of porous carbon.

3.5 Electrode design

The electrode structure also influences the electrochemical performances of SCs. An inherent microstructural trade-off between the ionic diffusion and electronic transport exists in the electrode materials. Note that pores or channels are conducive to effective ionic diffusion. Additionally, the connectivity of the carbon network with highly active reaction surface area promotes effective electronic transport.

For SCs, the design of the electrode structure could effectively boost comprehensive performances. In this respect, graphene can serve as both conductive agent and binder to replace conventional conductive agents, such as Ketjen black (KB), restricting the volume expansion of electrodes during charge/discharge processes of SCs[145, 146]. For instance, the introduction of graphene improves the electrochemical performances of activated carbon since graphene might support carbon particles and limit volume expansion. As shown in Fig. 11, the volume expanded by only 11% for graphene addition when compared to the sample prepared with KB addition (27%). Meanwhile, the former delivered better capacitance performance (173 $F \cdot g^{-1}$) than the latter (153 $F \cdot g^{-1}$)[147]. In graphene-cellulose paper (GCP) membranes, graphene acted as a binder to substitute the conventional PTFE or PVDF, comprising a novel three-dimensional interwoven structure of graphene nanosheets and cellulose fibers. This strategy is advantageous in terms of outstanding mechanical flexibility, excellent specific capacitance, high power performances, and long cycling stability when used as flexible, freestanding and binder-free SCs electrodes. The flexible GCP electrode delivered excellent areal capacitance of 81 $mF \cdot cm^{-2}$[148]. Additionally, the activated carbon particles could availably intercalate graphene

nanosheets to hinder stacking phenomena, thereby enhancing the effective ion-accessible surface area and promoting the ionic diffusion. Accordingly, binder-free composite electrodes made of reduced graphene oxide and activated carbon delivered high specific capacitance of 278 $F \cdot g^{-1}$ at 1 $mV \cdot s^{-1}$[149].

To enhance the capacitive performance and improve the cyclic stability, multi-dimensional graded electrodes with gradient PTFE distribution were constructed and exhibited excellent electrochemical properties (Fig. 12a). The capacitance of multi-dimensional (215 $F \cdot g^{-1}$) and radially-graded (208 $F \cdot g^{-1}$) elec-

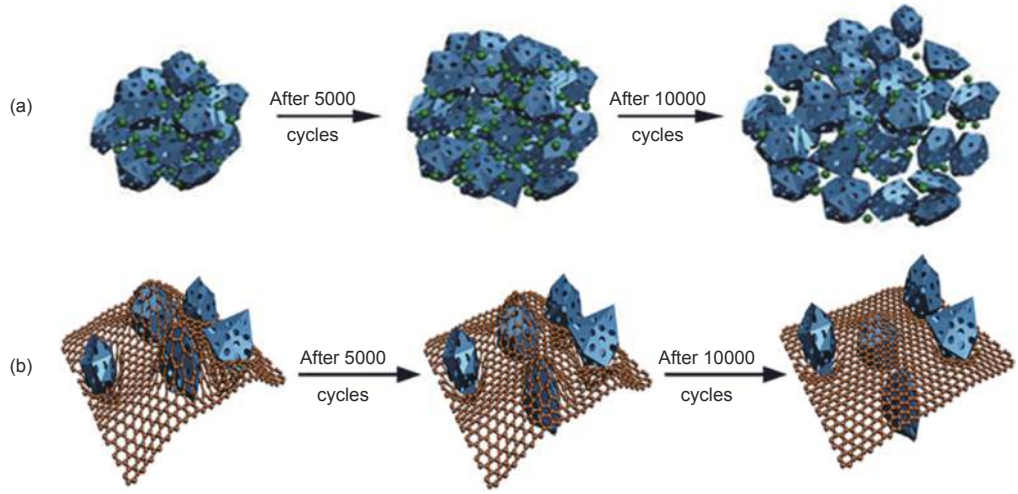

Fig. 11 Schematic diagrams of volume expansion in KB-AC (a) graphene-AC and (b) electrodes[147]. Reprinted with permission.

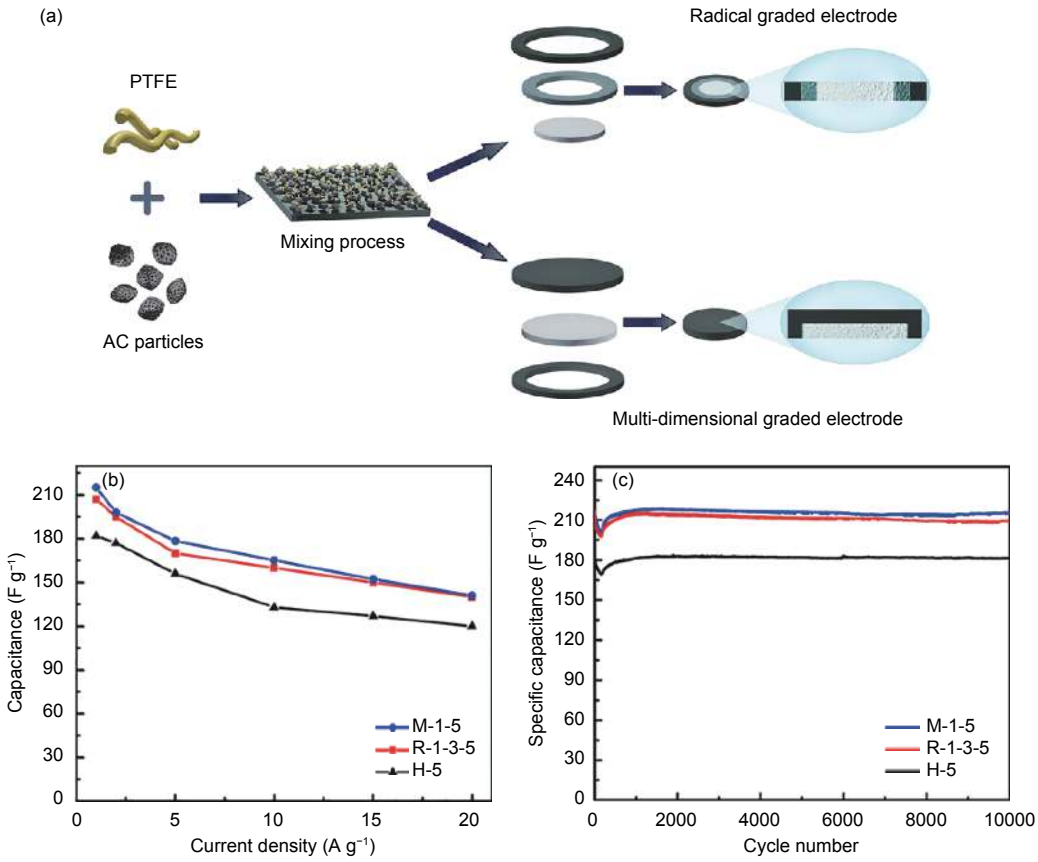

Fig. 12 (a) Schematic illustration of radial and multi-dimensional graded electrodes. Rate capability (b) cycling stability at 1 $A \cdot g^{-1}$ and (c) multi-dimensional graded, radical graded, and homogeneous electrodes in 6 mol/L KOH electrolyte[150]. Reprinted with permission.

trodes looked obviously better than the homogeneous electrodes (182 $F \cdot g^{-1}$) prepared with 5% PTFE (Fig. 12b). Note that lower PTFE contents did not decline the structural stability while higher PTFE contents blocked micropores and reduced the specific surface areas of electrodes. Also, multi-dimensional graded electrodes displayed superior capacitance retention of 99% (Fig. 12c). This results can be ascribed to the high PTFE concentration in the outer layer, which restricts the volumetric expansion and reduces the electrode cracking or pulverization during cycling[150].

4 Conclusions

This review demonstrated the importance of SCs as promising electrochemical energy storage devices due to their high-power densities, ultra-fast charge/discharge rates, long cyclic life services, and safe operation. The performances of porous carbon-based SCs are mainly influenced by the characteristics of porous carbon, such as the specific surface area, pore structure, surface heteroatoms, and structural defects. Desirable porous carbon should possess a high ion-accessible surface area and appropriate pore structure. A high ion-accessible surface area could provide abundant active sites for ions storage, while a porous structure may facilitate the storage and transport of ions, thereby influencing the specific capacitance and rate performance. Satisfactory pore size should match with the size of the desolvated ions for providing maximum capacitance and suitable numbers of transport channels for ions diffusion. In this perspective, the hierarchical porous structure could effectively improve both the energy density and power density of SCs. Thus, the pore structure should be considered when preparing or designing novel porous carbons. Accordingly, selecting appropriate probe gas and model is important for assessing the specific surface area and pore size distribution of porous carbons. Surface heteroatoms and structural defects also influence the electrochemical properties of porous carbons. The former enhances the wettability and electrical conductivity, as well as provides additional pseudocapacitance. By comparison, the latter induces substantial active sites for ions accumulation. Additionally, the rational electrode structure can further improve the electrode performance of the electrodes.

Although substantial progress has been made in porous carbon-based SCs, their comprehensive performances are still limited, especially in terms of low energy density required for practical applications. High-performance porous carbons still need further efforts. The charge storage mechanism and novel models of carbon-based SCs also require further development.

Acknowledgements

This work was supported by the National Natural Science Foundation of China (52062012), Key Science & Technology Project of Hainan Province (ZDYF2020028).

References

[1] Liu C, Li F, Ma L P, et al. Advanced materials for energy storage[J]. Advanced Materials, 2010, 22(8): E28-E62.

[2] Muzaffar A, Ahamed M B, Deshmukh K, et al. A review on recent advances in hybrid supercapacitors: Design, fabrication and applications[J]. Renewable & Sustainable Energy Reviews, 2019, 101: 123-145.

[3] Simon P, Gogotsi Y, Dunn B. Materials science. Where do batteries end and supercapacitors begin?[J]. Science, 2014, 343(6176): 1210-1211.

[4] Simon P, Gogotsi Y. Materials for electrochemical capacitors[J]. Nature Materials, 2008, 7(11): 845-854.

[5] Salanne M, Rotenberg B, Naoi K, et al. Efficient storage mechanisms for building better supercapacitors[J]. Nature Energy, 2016, 1(6): 16070.

[6] Zhang L L, Zhao X S. Carbon-based materials as supercapacitor electrodes[J]. Chemical Society Reviews, 2009, 38(9): 2520-2531.

[7] González A, Goikolea E, Barrena J A, et al. Review on supercapacitors: Technologies and materials[J]. Renewable and Sustainable Energy Reviews, 2016, 58: 1189-1206.

[8] Chen Y, Hao X, Chen G Z. Nanoporous versus nanoparticulate carbon-based materials for capacitive charge storage[J]. Energy & Environmental Materials, 2020, 3(3): 247-264.

[9] Shao H, Wu Y C, Lin Z, et al. Nanoporous carbon for electrochemical capacitive energy storage[J]. Chemical Society Reviews, 2020, 49(10): 3005-3039.

[10] Chmiola J, Yushin G, Gogotsi Y, et al. Anomalous increase in carbon capacitance at pore sizes less than 1 nanometer[J]. Science, 2006, 313(5794): 1760-1763.

[11] Largeot C, Portet C, Chmiola J, et al. Relation between the ion size and pore size for an electric double-layer capacitor[J]. Journal of the American Chemical Society, 2008, 130(9): 2730-2731.

[12] Jiang L L, Sheng L Z, Fan Z J. Biomass-derived carbon materials with structural diversities and their applications in energy storage[J]. Science China-Materials, 2018, 61(2): 133-158.

[13] Li Z J, Peng H N, Liu R R, et al. Quantitative assessment of basal-, edge- and defect-surfaces of carbonaceous materials and their influence on electric double-layer capacitance[J]. Journal of Power Sources, 2020, 457: 228022.

[14] Lyu L, Seong K d, Ko D, et al. Recent development of biomass-derived carbons and composites as electrode materials for supercapacitors[J]. Materials Chemistry Frontiers, 2019, 3(12): 2543-2570.

[15] Wang T, Zang X, Wang X, et al. Recent advances in fluorine-doped/fluorinated carbon-based materials for supercapacitors[J]. Energy Storage Materials, 2020, 30: 367-384.

[16] Li D H, Chang G J, Zong L, et al. From double-helix structured seaweed to S-doped carbon aerogel with ultra-high surface area for energy storage[J]. Energy Storage Materials, 2019, 17: 22-30.

[17] Li J M, Jiang Q M, Wei L S, et al. Simple and scalable synthesis of hierarchical porous carbon derived from cornstalk without pith for high capacitance and energy density[J]. Journal of Materials Chemistry A, 2020, 8(3): 1469-1479.

[18] Li J X, Han K H, Wang D, et al. Fabrication of high performance structural N-doped hierarchical porous carbon for supercapacitor[J]. Carbon, 2020, 164: 42-50.

[19] Zhu Y Y, Chen M M, Zhang Y, et al. A biomass-derived nitrogen-doped porous carbon for high-energy supercapacitor[J]. Carbon, 2018, 140: 404-412.

[20] Helmholtz H v. Ueber einige gesetze der vertheilung elektrischer strome in korperlichen leitern mit anwendung auf die thierisch-elektrischen versuche[J]. Annalen der Physik, 1853, 165: 211-233.

[21] Chapman D L. LI. A contribution to the theory of electrocapillarity[J]. The London, Edinburgh, and Dublin Philosophical Magazine and Journal of Science, 1913, 25(148): 475-481.

[22] Gouy M. Sur la constitution de la charge électrique à la surface d'un électrolyte[J]. Journal de Physique Théorique et Appliquée, 1910, 9(1): 457-468.

[23] Stern O. The theory of the electrolytic double-layer[J]. Z Elektrochem, 1924, 30: 508-516.

[24] Fedorov M V, Kornyshev A A. Ionic liquids at electrified interfaces[J]. Chemical Reviews, 2014, 114(5): 2978-3036.

[25] Bazant M Z, Storey B D, Kornyshev A A. Double layer in ionic liquids: Overscreening versus crowding[J]. Physical Review Letters, 2011, 106(4): 046102.

[26] Danish M, Ahmad T. A review on utilization of wood biomass as a sustainable precursor for activated carbon production and application[J]. Renewable and Sustainable Energy Reviews, 2018, 87: 1-21.

[27] He Y F, Zhuang X D, Lei C J, et al. Porous carbon nanosheets: Synthetic strategies and electrochemical energy related applications[J]. Nano Today, 2019, 24: 103-119.

[28] Shanmuga Priya M, Divya P, et al. A review status on characterization and electrochemical behaviour of biomass derived carbon materials for energy storage supercapacitors[J]. Sustainable Chemistry and Pharmacy, 2020, 16: 100243.

[29] Tang G X, Zhand L Q, Zhu X F, et al. The preparation of activated carbon from walnut shell bio-oil distillation residues[J]. New Carbon Materials, 2019, 34(5): 434-440.

[30] Wang J S, Zhang X, Li Z, et al. Recent progress of biomass-derived carbon materials for supercapacitors[J]. Journal of Power Sources, 2020, 451: 227794.

[31] Wei F, Zhang H F, He X J, et al. Synthesis of porous carbons from coal tar pitch for high-performance supercapacitors[J]. New Carbon Materials, 2019, 34(2): 132-139.

[32] Jia C, Li Y J, Yang Z, et al. Rich mesostructures derived from natural woods for solar steam generation[J]. Joule, 2017, 1(3): 588-599.

[33] Zhu M, Li Y, Chen G, et al. Tree-inspired design for high-efficiency water extraction[J]. Advanced Materials, 2017, 29(44): 1704107.

[34] Xiao C Y, Zhang W L, Lin H B, et al. Modification of a rice husk-based activated carbon by thermal treatment and its effect on its electrochemical performance as a supercapacitor electrode[J]. New Carbon Materials, 2019, 34(4): 341-348.

[35] Yang K, Peng J, Srinivasakannan C, et al. Preparation of high surface area activated carbon from coconut shells using microwave heating[J]. Bioresource Technology, 2010, 101(15): 6163-6169.

[36] Wang D H, Wang Y Z, Chen Y, et al. Coal tar pitch derived N-doped porous carbon nanosheets by the in-situ formed g-C_3N_4 as a template for supercapacitor electrodes[J]. Electrochimica Acta, 2018, 283: 132-140.

[37] Deng Y, Wei J, Sun Z, et al. Large-pore ordered mesoporous materials templated from non-Pluronic amphiphilic block copolymers[J]. Chemical Society Reviews, 2013, 42(9): 4054-4070.

[38] Lin Z, Liu S, Mao W, et al. Tunable self-assembly of diblock copolymers into colloidal particles with triply periodic minimal surfaces[J]. Angewandte Chemie-International Edition, 2017, 56(25): 7135-7140.

[39] Im U S, Kim J, Lee S H, et al. Preparation of activated carbon from needle coke via two-stage steam activation process[J]. Materials Letters, 2019, 237: 22-25.

[40] Qin L Y, Hou Z W, Lu S, et al. Porous carbon derived from pine nut shell prepared by steam activation for supercapacitor electrode material[J]. International Journal of Electrochemical Science, 2019, 14(9): 8907-8918.

[41] Lei E, Li W, Ma C H, et al. CO_2-activated porous self-templated N-doped carbon aerogel derived from banana for high-performance supercapacitors[J]. Applied Surface Science, 2018, 457: 477-486.

[42] Ma M J, Ying H J, Cao F F, et al. Adsorption of congo red on mesoporous activated carbon prepared by CO_2 physical activation[J]. Chinese Journal of Chemical Engineering, 2020, 28(4): 1069-1076.

[43] Chen W M, Luo M, Yang K, et al. Microwave-assisted KOH activation from lignin into hierarchically porous carbon with super high specific surface area by utilizing the dual roles of inorganic salts: Microwave absorber and porogen[J]. Microporous and Mesoporous Materials, 2020, 300: 110178.

[44] Zhu Z H, Liu Y J, Ju Z J, et al. Synthesis of diverse green carbon nanomaterials through fully utilizing biomass carbon source assisted by KOH[J]. ACS Applied Materials & Interfaces, 2019, 11(27): 24205-24211.

[45] Hu L F, Zhu Q Z, Wu Q, et al. Natural biomass-derived hierarchical porous carbon synthesized by an in situ hard template coupled with NaOH activation for ultrahigh rate supercapacitors[J]. ACS Sustainable Chemistry & Engineering, 2018, 6(11): 13949-13959.

[46] Zhang Y, Song X L, Xu Y, et al. Utilization of wheat bran for producing activated carbon with high specific surface area via NaOH activation using industrial furnace[J]. Journal of Cleaner Production, 2019, 210: 366-375.

[47] Chen H J, Wei H M, Fu N, et al. Nitrogen-doped porous carbon using $ZnCl_2$ as activating agent for high-performance supercapacitor electrode materials[J]. Journal of Materials Science, 2018, 53(4): 2669-2684.

[48] Sun Q J, Jiang T Y, Zhao G Z, et al. Porous carbon material based on biomass prepared by MgO template method and $ZnCl_2$ activation method as electrode for high performance supercapacitor[J]. International Journal of Electrochemical Science, 2019, 14(1): 1-14.

[49] Du W M, Zhang Z R, Du L G, et al. Designing synthesis of porous biomass carbon from wheat straw and the functionalizing application in flexible, all-solid-state supercapacitors[J]. Journal of Alloys and Compounds, 2019, 797: 1031-1040.

[50] Endo M, Maeda T, Takeda T, et al. Capacitance and pore-size distribution in aqueous and nonaqueous electrolytes using various activated carbon electrodes[J]. Journal of the Electrochemical Society, 2001, 148(8): A910-A914.

[51] Long C L, Chen X, Jiang L L, et al. Porous layer-stacking carbon derived from in-built template in biomass for high volumetric performance supercapacitors[J]. Nano Energy, 2015, 12: 141-151.

[52] J Gamby, Taberna P L, Simon P, et al. Studies and characterisations of various activated carbons used for carbon/carbon supercapacitors[J]. Journal of Power Sources, 2001, 101: 109-116.

[53] Linoam E, Gregory S, Abraham S, et al. Ion sieving effects in the electrical double layer of porous carbon electrodes: Estimating effective ion size in electrolytic solutions[J]. The Journal of Physical Chemistry B, 2001, 105: 6880-6887.

[54] Gregory S, Abraham S, Linoam E, et al. Carbon electrodes for double-layer capacitors I. Relations between ion and pore dimensions[J]. Journal of the Electrochemical Society, 2000, 147(7): 2486-2493.

[55] Raymundo-Piñero E, Kierzek K, Machnikowski J, et al. Relationship between the nanoporous texture of activated carbons and their capacitance properties in different electrolytes[J]. Carbon, 2006, 44(12): 2498-2507.

[56] Li Z, Gadipelli S, Li H, et al. Tuning the interlayer spacing of graphene laminate films for efficient pore utilization towards compact capacitive energy storage[J]. Nature Energy, 2020, 5(2): 160-168.

[57] Chmiola J, Largeot C, Taberna P L, et al. Desolvation of ions in subnanometer pores and its effect on capacitance and double-layer theory[J]. Angewandte Chemie-International Edition, 2008, 120(18): 3440-3443.

[58] Prehal C, Koczwara C, Jäckel N, et al. Quantification of ion confinement and desolvation in nanoporous carbon supercapacitors with modelling and in situ X-ray scattering[J]. Nature Energy, 2017, 2(3): 16215.

[59] Galhena D T, Bayer B C, Hofmann S, et al. Understanding capacitance variation in sub-nanometer pores by in situ tuning of interlayer constrictions[J]. ACS Nano, 2016, 10(1): 747-754.

[60] Tsai W Y, Taberna P L, Simon P. Electrochemical quartz crystal microbalance (EQCM) study of ion dynamics in nanoporous carbons[J]. Journal of the American Chemical Society, 2014, 136(24): 8722-8728.

[61] Jäckel N, Simon P, Gogotsi Y, et al. Increase in capacitance by subnanometer pores in carbon[J]. ACS Energy Letters, 2016, 1(6): 1262-1265.

[62] Kalluri R K, Konatham D, Striolo A. Aqueous NaCl solutions within charged carbon-slit pores: Partition coefficients and density distributions from molecular dynamics simulations[J]. The Journal of Physical Chemistry C, 2011, 115(28): 13786-13795.

[63] Liu H M, Jameson C J, Murad S. Molecular dynamics simulation of ion selectivity process in nanopores[J]. Molecular Simulation, 2008, 34(2): 169-175.

[64] Shao Q, Huang L L, Zhou J, et al. Molecular simulation study of temperature effect on ionic hydration in carbon nanotubes[J]. Physical Chemistry Chemical Physics, 2008, 10(14): 1896-1906.

[65] Kondrat S, Kornyshev A. Corrigendum: Superionic state in double-layer capacitors with nanoporous electrodes[J]. Journal of Physics: Condensed Matter, 2013, 25(11): 119501.

[66] Futamura R, Iiyama T, Takasaki Y, et al. Partial breaking of the Coulombic ordering of ionic liquids confined in carbon nanopores[J]. Nature Materials, 2017, 16(12): 1225-1232.

[67] Chmiola J, Yushin G, Dash R, et al. Effect of pore size and surface area of carbide derived carbons on specific capacitance[J]. Journal of Power Sources, 2006, 158(1): 765-772.

[68] Kondrat S, Pérez C R, Presser V, et al. Effect of pore size and its dispersity on the energy storage in nanoporous supercapacitors[J]. Energy & Environmental Science, 2012, 5(4): 6474-6479.

[69] Wang D W, Li F, Liu M, et al. Mesopore-aspect-ratio dependence of ion transport in rodtype ordered mesoporous carbon[J]. The Journal of Physical Chemistry C, 2008, 112(26): 9950-9955.

[70] Wang D W, Li F, Fang H T, et al. Effect of pore packing defects in 2-D ordered mesoporous carbons on ionic transport[J]. The Journal of Physical Chemistry B, 2006, 110(17): 8570-8575.

[71] Wang Q, Yan J, Fan Z J. Carbon materials for high volumetric performance supercapacitors: Design, progress, challenges and opportunities[J]. Energy & Environmental Science, 2016, 9(3): 729-762.

[72] Black J M, Andreas H A. Pore shape affects spontaneous charge redistribution in small pores[J]. The Journal of Physical

Chemistry C, 2010, 114(27): 12030-12038.
[73] Noked M, Avraham E, Soffer A, et al. The rate-determining step of electroadsorption processes into nanoporous carbon electrodes related to water desalination[J]. Journal of Physical Chemistry C, 2009, 113(51): 21319-21327.
[74] Kang X, Wang C, Yin J. Hierarchically porous carbons derived from cotton stalks for high-performance supercapacitors[J]. Chemelectrochem, 2017, 4(10): 2599-2607.
[75] Shang Z, An X Y, Zhang H, et al. Houttuynia-derived nitrogen-doped hierarchically porous carbon for high-performance supercapacitor[J]. Carbon, 2020, 161: 62-70.
[76] Shao R, Niu J, Liang J J, et al. Mesopore- and macropore-dominant nitrogen-doped hierarchically porous carbons for high-energy and ultrafast supercapacitors in non-aqueous electrolytes[J]. ACS Applied Materials & Interfaces, 2017, 9(49): 42797-42805.
[77] Wang D W, Li F, Liu M, et al. 3D aperiodic hierarchical porous graphitic carbon material for high-rate electrochemical capacitive energy storage[J]. Angewandte Chemie-International Edition, 2008, 47(2): 379-382.
[78] Xia L C, Huang H, Fan Z, et al. Hierarchical macro-/meso-/microporous oxygen-doped carbon derived from sodium alginate: A cost-effective biomass material for binder-free supercapacitors [J]. Materials & Design, 2019, 182: 108048.
[79] Zhang Q, Han K, Li S, et al. Synthesis of garlic skin-derived 3D hierarchical porous carbon for high-performance supercapacitors [J]. Nanoscale, 2018, 10(5): 2427-2437.
[80] Zhi L, Li T, Yu H, et al. Hierarchical graphene network sandwiched by a thin carbon layer for capacitive energy storage[J]. Carbon, 2017, 113: 100-107.
[81] Huang J, Sumpter B G, Meunier V, et al. Curvature effects in carbon nanomaterials: Exohedral versus endohedral supercapacitors[J]. Journal of Materials Research, 2011, 25(8): 1525-1531.
[82] Huang J, Sumpter B G, Meunier V. Theoretical model for nanoporous carbon supercapacitors[J]. Angewandte Chemie-International Edtion, 2008, 47(3): 520-524.
[83] Huang J, Sumpter B G, Meunier V. A universal model for nanoporous carbon supercapacitors applicable to diverse pore regimes, carbon materials and electrolytes[J]. Chemistry-A European Journal, 2008, 14(22): 6614-6626.
[84] Feng G, Qiao R, Huang J, et al. Ion distribution in electrified micropores and its role in the anomalous enhancement of capacitance[J]. ACS Nano, 2010, 4(4): 2382-2390.
[85] Thommes M, Cychosz K A. Physical adsorption characterization of nanoporous materials: Progress and challenges[J]. Adsorption-Journal of the International Adsorption Society, 2014, 20: 233-250.
[86] Sing K S W, Williams R T. The use of molecular probes for the characterization of nanoporous adsorbents[J]. Particle & Particle Systems Characterization, 2004, 21(2): 71-79.
[87] Silvestre-Albero J, Silvestre-Albero A, Rodríguez-Reinoso F, et al. Physical characterization of activated carbons with narrow microporosity by nitrogen (77.4 K), carbon dioxide (273 K) and argon (87.3 K) adsorption in combination with immersion calorimetry[J]. Carbon, 2012, 50(9): 3128-3133.
[88] García-Martínez J, Cazorla-Amorós D, Linares-Solano A. Further evidences of the usefulness of CO_2 microporous solids.[J]. Studies in Surface Science and Catalysis, 2000, 128: 485-494.
[89] Furmaniak S, Terzyk A P, Gauden P A, et al. The influence of carbon surface oxygen groups on Dubinin-Astakhov equation parameters calculated from CO_2 adsorption isotherm[J]. Journal of Physics-Condensed Matter, 2010, 22(8): 085003.
[90] Zhang Z, Yang Z. Theoretical and practical discussion of measurement accuracy for physisorption with micro- and mesoporous materials[J]. Chinese Journal of Catalysis, 2013, 34(10): 1797-1810.
[91] Rouquerol J, Llewellyn P, Rouquerol F. Is the BET equation applicable to microporous adsorbents?[J]. Studies in Surface Science and Catalysis, 2007, 160: 49-56.
[92] Barrett E P, Joyner L G, Halenda P P. The determination of pore volume and area distributions in porous substances. I. Computations from nitrogen isotherms[J]. Journal of the American Chemical Society, 1951, 73(1): 373-380.
[93] Dubinin M M, Polyakov N S, Kataeva L I. Basic properties of equations for physical vapor adsorption in micropores of carbon adsorbents assuming a normal micropore distribution[J]. Carbon, 1991, 29: 481-488.
[94] Dubinin M M. The potential theory of adsorption of gases and vapors for adsorbents with energetically nonuniform surfaces[J]. Chemical Reviews, 1960, 60: 235-241.
[95] Horvath G, Kawazoe, K. Method for the calculation of effective pore size distribution in molecular sieve carbon[J]. Journal of Chemical Engineering of Japan, 1983, 16: 470-475.
[96] Saito A, Foley H C. Curvature and parametric sensitivity in models for adsorption in micropores[J]. Aiche Journal, 1991, 37(3): 429-436.
[97] Thommes M, Köhn R, Fröba M. Sorption and pore condensation behavior of nitrogen, argon, and krypton in mesoporous MCM-48 silica materials[J]. The Journal of Physical Chemistry B, 2000, 104(33): 7932-7943.
[98] Ravikovitch P I, Neimark A V. Density functional theory model of adsorption deformation[J]. Langmuir, 2006, 22(26): 10864-10868.
[99] Tarazona P, Marconi U M B, Evans R. Phase equilibria of fluid interfaces and confined fluids[J]. Molecular Physics, 1987, 60(3): 573-595.
[100] Gor G Y, Thommes M, Cychosz K A, et al. Quenched solid density functional theory method for characterization of mesoporous carbons by nitrogen adsorption[J]. Carbon, 2012, 50(4): 1583-1590.
[101] Ravikovitch P I, Neimark A V. Density functional theory model of adsorption on amorphous and microporous silica materials[J]. Langmuir, 2006, 22(26): 11171-11179.
[102] Jagiello J, Olivier J P. 2D-NLDFT adsorption models for carbon slit-shaped pores with surface energetical heterogeneity and geometrical corrugation[J]. Carbon, 2013, 55: 70-80.
[103] Kwiatkowski M, Fierro V, Celzard A. Confrontation of various adsorption models for assessing the porous structure of activated carbons[J]. Adsorption-Journal of the International Adsorption

Society, 2019, 25(8): 1673-1682.

[104] Lai W D, Yang S, Jiang Y H, et al. Artefact peaks of pore size distributions caused by unclosed sorption isotherm and tensile strength effect[J]. Adsorption-Journal of the International Adsorption Society, 2020, 26(4): 633-644.

[105] Niu J, Shao R, Liang J J, et al. Biomass-derived mesopore-dominant porous carbons with large specific surface area and high defect density as high performance electrode materials for Li-ion batteries and supercapacitors[J]. Nano Energy, 2017, 36: 322-330.

[106] Banks C E, Davies T J, Wildgoose G G, et al. Electrocatalysis at graphite and carbon nanotube modified electrodes: Edge-plane sites and tube ends are the reactive sites[J]. Chemical Communications, 2005(7): 829-841.

[107] Kim T, Lim S, Kwon K, et al. Electrochemical capacitances of well-defined carbon surfaces[J]. Langmuir, 2006, 22(22): 9086-9088.

[108] Qu D. Studies of the activated carbons used in double-layer supercapacitors[J]. Journal of Power Sources, 2002, 109(2): 403-411.

[109] Yuan W, Zhou Y, Li Y, et al. The edge- and basal-plane-specific electrochemistry of a single-layer graphene sheet[J]. Scientific Reports, 2013, 3: 2248.

[110] Lu Q J, Zhou S Q, Li B, et al. Mesopore-rich carbon flakes derived from lotus leaves and it's ultrahigh performance for supercapacitors[J]. Electrochimica Acta, 2020, 333: 135481.

[111] Yan X C, Jia Y, Zhuang L Z, et al. Defective carbons derived from Macadamia nut shell biomass for efficient oxygen reduction and supercapacitors[J]. Chemelectrochem, 2018, 5(14): 1874-1879.

[112] Nath N C D, Shah S S, Qasem M A A, et al. Defective carbon nanosheets derived from syzygium cumini leaves for electrochemical energy-storage[J]. Chemistryselect, 2019, 4(31): 9079-9083.

[113] Welham N J, Berbenni V, Chapman P G. Effect of extended ball milling on graphite[J]. Journal of Alloys and Compounds, 2003, 349(1-2): 255-263.

[114] Yue X, Wang H, Wang S, et al. In-plane defects produced by ball-milling of expanded graphite[J]. Journal of Alloys and Compounds, 2010, 505(1): 286-290.

[115] Dong Y, Lin X, Wang D, et al. Modulating the defects of graphene blocks by ball-milling for ultrahigh gravimetric and volumetric performance and fast sodium storage[J]. Energy Storage Materials, 2020, 30: 287-295.

[116] Abioye A M, Ani F N. Recent development in the production of activated carbon electrodes from agricultural waste biomass for supercapacitors: A review[J]. Renewable & Sustainable Energy Reviews, 2015, 52: 1282-1293.

[117] Sun K L, Yu S S, Hu Z L, et al. Oxygen-containing hierarchically porous carbon materials derived from wild jujube pit for high-performance supercapacitor[J]. Electrochimica Acta, 2017, 231: 417-428.

[118] Zhao N, Deng L B, Luo D W, et al. Oxygen doped hierarchically porous carbon for electrochemical supercapacitor[J]. International Journal of Electrochemical Science, 2018, 13(11): 10626-10634.

[119] Liu M C, Kong L B, Zhang P, et al. Porous wood carbon monolith for high-performance supercapacitors[J]. Electrochimica Acta, 2012, 60: 443-448.

[120] Wang D W, Li F, Liu M, et al. Improved capacitance of SBA-15 templated mesoporous carbons after modification with nitric acid oxidation[J]. New Carbon Materials, 2007, 22(4): 307-314.

[121] Li X R, Jiang Y H, Wang P Z, et al. Effect of the oxygen functional groups of activated carbon on its electrochemical performance for supercapacitors[J]. New Carbon Materials, 2020, 35(3): 232-243.

[122] Sahoo G, Polaki S R, Ghosh S, et al. Plasma-tuneable oxygen functionalization of vertical graphenes enhance electrochemical capacitor performance[J]. Energy Storage Materials, 2018, 14: 297-305.

[123] Jiang L L, Sheng L Z, Long C L, et al. Functional pillared graphene frameworks for ultrahigh volumetric performance supercapacitors[J]. Advanced Energy Materials, 2015, 5(15): 1500771.

[124] Anjos D M, McDonough J K, Perre E, et al. Pseudocapacitance and performance stability of quinone-coated carbon onions[J]. Nano Energy, 2013, 2(5): 702-712.

[125] Yuan S, Huang X, Wang H, et al. Structure evolution of oxygen removal from porous carbon for optimizing supercapacitor performance[J]. Journal of Energy Chemistry, 2020, 51: 396-404.

[126] Shen W, Fan W. Nitrogen-containing porous carbons: Synthesis and application[J]. Journal of Materials Chemistry A, 2013, 1(4): 999-1013.

[127] Wei W, Chen Z, Zhang Y, et al. Full-faradaic-active nitrogen species doping enables high-energy-density carbon-based supercapacitor[J]. Journal of Energy Chemistry, 2020, 48: 277-284.

[128] Lin L, Xie H M, Lei Y, et al. Nitrogen source-mediated cocoon silk-derived N, O-doped porous carbons for high performance symmetric supercapacitor[J]. Journal of Materials Science-Materials in Electronics, 2020, 31(13): 10825-10835.

[129] Guo J, Wu D L, Wang T, et al. P-doped hierarchical porous carbon aerogels derived from phenolic resins for high performance supercapacitor[J]. Applied Surface Science, 2019, 475: 56-66.

[130] Jin H, Feng X, Li J, et al. Heteroatom-doped porous carbon materials with unprecedented high volumetric capacitive performance[J]. Angewandte Chemie-Internation Edition, 2019, 58(8): 2397-2401.

[131] Zhou J, Lian J, Hou L, et al. Ultrahigh volumetric capacitance and cyclic stability of fluorine and nitrogen co-doped carbon microspheres[J]. Nature Communications, 2015, 6: 8503.

[132] Zhou J, Xu L, Li L, et al. Polytetrafluoroethylene-assisted N/F co-doped hierarchically porous carbon as a high performance electrode for supercapacitors[J]. Journal of Colloid and Interface Science, 2019, 545: 25-34.

[133] Guo H L, Gao Q M. Boron and nitrogen co-doped porous carbon and its enhanced properties as supercapacitor[J]. Journal of Power Sources, 2009, 186(2): 551-556.

[134] Wang Y K, Zhang M K, Dai Y, et al. Nitrogen and phosphorus co-doped silkworm-cocoon-based self-activated porous carbon for high performance supercapacitors[J]. Journal of Power Sources, 2019, 438: 227045.

[135] Huo S L, Zhao Y B, Zong M Z, et al. Boosting supercapacitor and capacitive deionization performance of hierarchically porous carbon by polar surface and structural engineering[J]. Journal of Materials Chemistry A, 2020, 8(5): 2505-2517.
[136] Ren G Y, Li Y N, Chen Q S, et al. Sepia-derived N, P co-doped porous carbon spheres as oxygen reduction reaction electrocatalyst and supercapacitor[J]. ACS Sustainable Chemistry & Engineering, 2018, 6(12): 16032-16038.
[137] Tang B, Zheng L P, Dai X C, et al. Nitrogen/oxygen co-doped porous carbons derived from a facilely-synthesized Schiff-base polymer for high-performance supercapacitor[J]. Journal of Energy Storage, 2019, 26: 100961.
[138] Wang P Z, Luo W X, Guo N N, et al. Nitrogen and oxygen co-doped hierarchical porous carbon for high performance supercapacitor electrodes[J]. Chemical Physics Letters, 2019, 730: 32-38.
[139] Jia S, Wei J, Meng X T, et al. Facile and friendly preparation of N/S Co-doped graphene-like carbon nanosheets with hierarchical pore by molten salt for all-solid-state supercapacitor[J]. Electrochimica Acta, 2020, 331: 135338.
[140] Ping Y J, Han J Z, Li J J, et al. N, S co-doped porous carbons from natural Juncus effuses for high performance supercapacitors[J]. Diamond and Related Materials, 2019, 100: 107577.
[141] Na W, Jun J, Park J W, et al. Highly porous carbon nanofibers co-doped with fluorine and nitrogen for outstanding supercapacitor performance[J]. Journal of Materials Chemistry A, 2017, 5(33): 17379-17387.
[142] Ling Z, Wang Z Y, Zhang M D, et al. Sustainable synthesis and assembly of biomass-derived B/N co-doped carbon nanosheets with ultrahigh aspect ratio for high-performance supercapacitors[J]. Advanced Functional Materials, 2016, 26(1): 111-119.
[143] Zhao Z C, Xie Y B. Electrochemical supercapacitor performance of boron and nitrogen co-doped porous carbon nanowires[J]. Journal of Power Sources, 2018, 400: 264-276.
[144] Wang C S, Liu T Z. Nori-based N, O, S, Cl co-doped carbon materials by chemical activation of $ZnCl_2$ for supercapacitor[J]. Journal of Alloys and Compounds, 2017, 696: 42-50.
[145] Choi J H, Kim Y, Kim B S. Multifunctional role of reduced graphene oxide binder for high performance supercapacitor with commercial-level mass loading[J]. Journal of Power Sources, 2020, 454: 227917.
[146] Xu B, Wang H, Zhu Q, et al. Reduced graphene oxide as a multi-functional conductive binder for supercapacitor electrodes[J]. Energy Storage Materials, 2018, 12: 128-136.
[147] Yang S, Zhao F Y, Li X R, et al. Electrode structural changes and their effects on capacitance performance during preparation and charge-discharge processes[J]. Journal of Energy Storage, 2019, 24: 100799.
[148] Weng Z, Su Y, Wang D W, et al. Graphene-cellulose paper flexible supercapacitors[J]. Advanced Energy Materials, 2011, 1(5): 917-922.
[149] Liu C X, Chen J, Zhang C F, et al. Facile preparation of binder free electrode for electrochemical capacitors based on reduced graphene oxide composite film[J]. Journal of Electroanalytical Chemistry, 2019, 847: 113133.
[150] Zhang X R, Yang S, Jiang Y H, et al. Multi-dimensional graded electrodes with enhanced capacitance and superior cyclic stability[J]. Journal of Power Sources, 2021, 481: 228911.

多孔炭对超级电容器电荷存储的影响

罗先游[1,2]， 陈 永[1,2,*]， 莫 岩[2,*]

（1. 佛山科学技术学院 材料科学与氢能学院，广东 佛山 528000；
2. 海南大学 南海海洋资源利用国家重点实验室，海南省硅锆钛资源利用研究省重点实验室，海南 海口 570228）

摘 要： 由于具有良好的物理化学稳定性、高比表面积、可调的孔结构及优良的导电性，多孔炭广泛应用于超级电容器电极材料。它的电容性能与其比表面积、孔结构、表面杂原子、结构缺陷及电极结构密切相关。离子及表面积（有效表面）能够提供丰富的活性位点，而合适的孔结构有利于离子的传输和存储，因而共同影响着炭基电极材料的比电容和倍率性能。具有合适孔径分布、一定数量的离子传输通道及微孔/介孔比例，是提高超级电容器能量密度和功率密度的必要条件。此外，结构缺陷、表面杂原子及合理的电极结构设计对多孔炭基超级电容器的电容性能具有重要的影响。

关键词： 超级电容器；多孔炭；比表面积；孔结构；电极结构

文章编号： 1007-8827(2021)01-0049-20 **中图分类号：** TQ127.1+1 **文献标识码：** A

基金项目： 国家自然科学基金 (52062012)；海南省重点研发项目 (ZDYF2020028).

通讯作者： 陈 永，博士，教授. E-mail: ychen2002@163.com；
莫 岩，博士. E-mail: myfriends66@163.com

作者简介： 罗先游，博士研究生. E-mail: luoxianyou1990@163.com

本文的电子版全文由 Elsevier 出版社在 ScienceDirect 上出版（http://www.sciencedirect.com/science/journal/18725805）